Theory of the electronic properties of δ-doped layers with DX centers in semiconductor heterostructures

M. E. Lazzouni and L. J. Sham
Department of Physics 0350, University of California, San Diego, 9500 Gilman Drive, La Jolla, California 92093-0350
(Received 22 June 1992; revised manuscript received 26 October 1992)

We attempt to build a flexible and accurate theoretical model for the electronic properties of selectively doped semiconductor heterostructures based on a two-band $\mathbf{k}\cdot\mathbf{p}$ effective-mass-approximation Hamiltonian that includes nonparabolicity, stress, piezoelectric, finite-temperature, many-body, and DX-center effects. We present quantitative self-consistent results for a variety of δ-modulation-doped semiconductor heterostructures with the aim of optimizing the electronic density in the active region as a function of configuration, including [001] and [111] interfaces for device applications. The presence of DX centers leads to the prediction of saturation of the carrier density with a characteristic capacitance discontinuity as the δ-doping concentration is increased. Calculated differential capacitance C-V curves indicate that spatial charge-density inhomogeneities, but not subband depopulation, lead to sharp steps in the capacitance as the gate voltage is increased.

I. INTRODUCTION

The advances in epitaxial growth techniques such as molecular-beam epitaxy (MBE) have made it possible to grow semiconductor heterostructures of high quality, whose configuration can be tailored to a variety of desired specifications.[1] Various doping profiles can be inserted with great flexibility in these structures, notably the doping impurities can be inserted within a monolayer of the semiconductor materials resulting in what is commonly referred to as δ doping.[2] Theories have been given of the electronic properties in the presence of δ doping in devices.[3] Experimental groups are taking advantage of these advances in materials preparation to design and construct heterostructure electronic devices with better performance. The purpose of this paper is to provide a theoretical guide for such designs. We restrict ourselves here to planar structures. The two factors most connected with the performance of the device are the carrier mobility and the carrier density.[4] We shall concentrate on the carrier-density distribution, particularly the carrier concentration in the conducting channel, and the possibility of undesirable parallel conduction. For devices operating at room temperature, the density is a better subject for design control than conductance. Our aim is to develop a flexible theoretical model which can treat any planar configuration of heterostructures and which includes all the important factors that affect quantitatively the calculation of the electron-density distribution, including the doping impurity configuration, DX centers, band nonparabolicity, stress, piezoelectric effect, finite temperature, and electron-electron interaction effects. In this paper we present such a model and use it to study the density distribution, the electronic states, conduction-band edge profile, and other related quantities as a function of various configurations which are important from the device application standpoint. First, a comparison with available experimental data in δ-doped GaAs is made to assess the accuracy of the theory. Then it is used to generate quantitative results of the electronic properties of δ-modulation-doped heterostructures as a function of configuration, with one or two δ layers, with uniform doping, or for a parabolic well.

In theoretical studies of the electronic properties in the conduction band of the heterostructures, the self-consistent solutions of the one-band effective-mass Schrödinger equation and the Poisson equation are commonly used.[4] However, the energy of the relevant electron is often far enough away from the conduction-band edges in the well regions and in the barrier regions that the parabolic dispersion is inaccurate.[5] We follow Ref. 5 in using the two-band $\mathbf{k}\cdot\mathbf{p}$ model[6] which takes into account the nonparabolic corrections in a simple and effective manner. The Schrödinger-like effective-mass equation obtained is solved self-consistently with the Poisson equation providing the Hartree approximation. The exchange-correlation effects are taken into account in the local-density approximation (LDA) of the density-functional theory.[7] The effects of applied gate voltages are accounted for in the boundary conditions of the Poisson equation.

To maintain the flexibility of the configuration design, we do not require the layers to be lattice matched. The electronic properties are then greatly influenced by the strain effects.[8] The two-band model allows the treatment of the strain effects in a systematic manner.

To confine the carriers in the conduction channel, it is desirable to use a large-gap semiconductor for the barrier. Then the conduction-band edge tends to be at the X point or has energy close to the X valley. In those circumstances, DX centers[9] appear, when doping impurities of group IV are introduced in the barrier III-V semiconductor, producing deep donor levels. The effects of DX centers on device performance prompts intensive experimental studies of the DX centers[10] and have been included in theoretical calculations of the electronic properties.[11,12] Reference 11 mentioned the inclusion of deep donors in

$Al_xGa_{1-x}As$ in their study of the quantum dot without describing the effects of the donors. Reference 12 treated the electron motion classically but, nonetheless, produced useful insight into the effects of the deep donors on the device conductance. We use the Chadi-Chang model[13] for the DX centers in order to study quantitatively the amount of donor ionization into electrons in the conduction channel.

Capacitance versus gate-voltage measurements provide a common and important experimental tool to infer the electronic distribution in doped semiconductor heterostructures in general[14] and in δ-doped structures in particular.[3] It has been suggested[15] that in wide parabolic quantum wells the C-V curves that present steplike changes with increasing gate voltage are indicative of the well subbands depopulation, although in a more recent experiment[16] the steplike changes have been interpreted as due to spatial inhomogeneities in electron density. The capacitance is a measure of a small change of electron-density distribution corresponding to a small change in gate voltage. Numerical differentiation of the density distribution at two close voltages is fraught with danger of misinterpreting numerical errors as physical structures in the C-V curve. We present an analytical formulation of the change in density distribution to first order in the change in gate voltage by the first-order perturbation theory of the self-consistent effective-mass equation. The numerical evaluation of the C-V curves in these structures then avoids the artificial structures of the numerical differentiation. We use our method to calculate the C-V curves of the δ-modulation-doped heterostructures as well as parabolic quantum wells with and without a superlattice superimposed.

The paper is organized as follows. In Sec. II the theory of electronic properties in arbitrary planar heterostructures is presented in some detail. Section III is devoted to the theory of capacitance calculation. In Sec. IV we present our numerical results for the electronic properties of a number of heterostructure configurations and compare them where possible with experiments. We conclude in the final section with a summary of the important results made possible by our theory and with a sketch of possible future applications of our theory.

II. THEORETICAL MODEL

A. Hamiltonian with strain

We choose to use the two-band effective-mass model including the conduction band and the degenerate valence bands as the most convenient way to account for the deviation from parabolicity when the electron energy is not close to the conduction-band edge of either the barrier[5] or the well. Also, when the heterostructures are made of lattice mismatched materials and the layers are thin enough, the mismatch can be accommodated by lattice strain.[8] We include the strain effects through the following Hamiltonian term:[17]

$$\begin{aligned} H_\epsilon^{(i)} = & -a^{(i)}[\epsilon_{xx}+\epsilon_{yy}+\epsilon_{zz}] \\ & -3b^{(i)}[(L_x^2-\tfrac{1}{3}L^2)\epsilon_{xx}+\text{c.p.}] \\ & -\frac{6}{\sqrt{3}}d^{(i)}[\{L_xL_y\}\epsilon_{xy}+\text{c.p.}], \end{aligned} \tag{1}$$

where c.p. denotes cyclic permutation with respect to x, y, and z, where $a^{(i)}$ is the hydrostatic deformation potential, $b^{(i)}$ and $d^{(i)}$ are shear deformation potentials appropriate to strains of tetragonal and rhombohedral symmetries, respectively, ϵ_{jk} is the strain tensor, the superscript (i) is a band index, which takes the value zero in the conduction band of s symmetry and one in the valence band of p symmetry, L_i is the corresponding orbital angular-momentum matrix, and $\{L_iL_j\}$ represents the symmetrized product. We restrict our attention to the binary and ternary III-V compounds and use atomic units everywhere in this paper. The Hamiltonian is taken to be the sum of the strain Hamiltonian and the two-band $\mathbf{k}\cdot\mathbf{p}$ model neglecting the spin-orbit interaction and the quadratic terms in k. The Schrödinger equation including strain effects has the form

$$\begin{pmatrix} V+\Delta+\frac{\delta E_g}{2}-E & Pk_x & Pk_y & -iPd/dz \\ Pk_x & V-\Delta-\frac{\delta E_g}{2}-E & 0 & 0 \\ Pk_y & 0 & V-\Delta-\frac{\delta E_g}{2}-E & 0 \\ -iPd/dz & 0 & 0 & V-\Delta-\frac{\delta E_g}{2}-\delta V_b-E \end{pmatrix} \begin{pmatrix} \psi \\ \phi_x \\ \phi_y \\ \phi_z \end{pmatrix} = 0, \tag{2}$$

where 2Δ represents the bulk unstrained band gap, ψ, ϕ_x, ϕ_y, and ϕ_z are components of the envelope function, and

$$\delta E_g = \left[-2a\frac{C_{11}-C_{12}}{C_{11}} + b\frac{C_{11}+2C_{12}}{C_{11}}\right]\epsilon, \tag{3a}$$

$$\delta V_b = -3b\frac{C_{11}+2C_{12}}{C_{11}}\epsilon, \tag{3b}$$

if the growth direction is taken along the [001] axis and

$$\delta E_g = \left[-3a\frac{C_{12}+4C_{44}}{C_{11}+2C_{12}+4C_{44}} + \sqrt{3}d\frac{C_{11}+C_{12}}{C_{11}+2C_{12}+4C_{44}}\right]\epsilon, \tag{4a}$$

$$\delta V_b = -3\sqrt{3}d\frac{C_{11}+C_{12}}{C_{11}+2C12+4C_{44}}\epsilon, \tag{4b}$$

if the growth direction is taken along the [111] axis. Here a without the superscript band index denotes the differ-

ence between the hydrostatic deformation potentials of the conduction and valence bands, b and d without the superscript band index denote shear deformation potentials in the valence band appropriate to strains of tetragonal and rhombohedral symmetries, respectively, and

$$\epsilon = -\frac{a_0 - a}{a}, \tag{5}$$

where a and a_0 are the unstrained and strained lattice constants of the materials, respectively. When structures grown on thick GaAs or InP substrates are considered, a_0 is taken to be the lattice constant of GaAs or InP. The C_{ij} are the elastic constants.

If we take the reference of energy at the bottom of the conduction band of the material with the smallest band gap, the system of Eqs. (2) leads, by elimination of ϕ_x, ϕ_y, and ϕ_z, to the following Schrödinger-like equation:

$$\left[-\frac{1}{2}\frac{d}{dz}\frac{1}{m_{\|}(z,E_i)}\frac{d}{dz} + \frac{k_x^2 + k_y^2}{2m_{\perp}(z,E_i)} + V(z) - E_i\right]\psi_i = 0, \tag{6}$$

where z is along the growth direction, the transverse mass is given by

$$m_{\perp}(z,E_i) = m'^{*}(z)\left(1 + \frac{E_i - V(z)}{2\Delta'}\right), \tag{7}$$

and the longitudinal mass by

$$m_{\|}(z,E_i) = m'^{*}(z)\left(1 + \frac{E_i - V(z) + \delta V_b}{2\Delta'}\right), \tag{8}$$

where

$$\Delta' = \Delta + \frac{\delta E_g}{2}, \tag{9}$$

and $m'^{*}(z) = \Delta'(z)/P^2$. Therefore, the strain affects Eq. (6) in two ways: First, it alters the value of the mass, through Δ', increasing it for the compressed materials and decreasing it for the dilated ones. Second, it leads to different masses in the parallel and normal directions to the growth axis due to the change in the cubic symmetry, since the term δV_b appears only in the longitudinal mass. The potential $V(z)$ is given by

$$V(z) = V_s(z) + V_H(z) + V_{\mathrm{XC}}(z). \tag{10}$$

$V_s(z)$ is the conduction-band-edge potential of the undoped heterostructure. $V_H(z)$ is the Hartree energy due to the doping impurities and the mobile electrons, whose densities are taken to be $\rho_d(z)$ and $\rho(z)$, respectively. $V_H(z)$ satisfies the Poisson equation

$$\frac{d}{dz}\epsilon(z)\frac{dV_H(z)}{dz} = 4\pi[\rho_d(z) - \rho(z)], \tag{11}$$

$\epsilon(z)$ being the dielectric constant. $V_{\mathrm{XC}}(z)$ is the LDA exchange-correlation potential. We have chosen to use the expression parametrized by Perdew and Zunger[18] using the local mass and dielectric constant. The energy dependence in the masses is a consequence of the two-band model which provides a mechanism for deviation of the conduction band from parabolicity. The mobile electron density is given by

$$\rho(z) = 2\sum_{E_i} f(E_i)\psi_i^2(z), \tag{12}$$

where $f(E_i)$ is the Fermi-Dirac distribution function, and the factor 2 is due to spin.

In addition, we have to take into account the piezoelectric nature of the materials. Since in this case only the piezoelectric constant e_{14} is nonzero, the diagonal strains do not induce any polarization. However, the [111]-grown structures[19] have finite off-diagonal strain components that generate an electric polarization parallel to the growth direction given by

$$P_z^s = \sqrt{3}e_{14}\epsilon_{xz}. \tag{13}$$

The displacement field in the Maxwell equations becomes

$$\mathbf{D} = \mathbf{E} + 4\pi\mathbf{P}^s, \tag{14}$$

where $\mathbf{E}$ is the electric field. The Poisson equation acquires a new term given by $4\pi\frac{dP_z^s}{dz}$ which is nonvanishing at the interfaces. This term will act as a dipole whose energy must be added to the potential $V(z)$ in the Schrödinger-like equation.

From Eq. (6) we see that the boundary conditions for the envelope functions are that ψ_i and

$$\frac{1}{m_{\|}(z,E_i)}\frac{d}{dz}\psi_i \tag{15}$$

are continuous[5], since V(z) is at worst piecewise continuous. The one-band model is recovered if we neglect the quantity $\epsilon = [E_i - V(z)]/2\Delta'(z)$ in Eq. (6).

The boundary conditions for the Poisson equation (11) depend on the specific structure we are studying. In the calculations we performed, we encountered two cases. The first is the isolated structures, where from charge neutrality the boundary conditions are that the electric field $dV_H(z)/dz$ is zero at both ends of the structure. The second is the case where the structures are between an Ohmic contact or a semi-insulating substrate and a Schottky barrier. Then we take $V_H(0) = V_0$, the energy at the top of the Schottky barrier, and $V_H(z)$ and $dV_H(z)/dz$ to be equal zero at the other end. We use the first condition to determine the Fermi energy and the other two to integrate the Poisson equation.

B. Numerical procedure

We seek a self-consistent solution to Eqs. (6) and (11). We can simplify this problem significantly if we make the following approximation. We see that the eigenenergy E_i is a function of $k^2 = k_x^2 + k_y^2$. Since we are dealing with energies close to the conduction-band edge we can expand E_i to first order in k^2

$$E_i(k^2) = E_i^{(0)} + \frac{k^2}{2m_i^*}, \tag{16}$$

where m_i^* is a parallel mass introduced to simplify the k^2 integration in the electronic density. Then Eq. (6) to first order in k^2 becomes

$$\left[-\frac{1}{2}\frac{d}{dz}\frac{1}{m_{\|}(z,E_i^{(0)})}\frac{d}{dz} + \frac{k^2}{2m_{\perp}(z,E_i^{(0)})} + V(z) + \frac{k^2}{2m_i^*}\frac{d}{dz}\frac{m'^*(z)}{4m_{\|}(z,E_i^{(0)})^2\Delta'(z)}\frac{d}{dz} - E_i^{(0)} - \frac{k^2}{2m_i^*}\right]\psi_i = 0. \tag{17}$$

It is a reasonable approximation by first-order perturbation theory[20] to eliminate the k^2 term in this equation by choosing m_i^* as

$$m_i^* = \frac{1 - \frac{1}{4}\left\langle \psi_i \left| \frac{d}{dz}\frac{m'^*(z)}{m_{\|}(z,E_i^{(0)})^2\Delta'(z)}\frac{d}{dz} \right| \psi_i \right\rangle}{\left\langle \psi_i \left| \frac{1}{m_{\perp}(z,E_i^{(0)})} \right| \psi_i \right\rangle} \tag{18}$$

as long as the masses do not vary too much with z, which is the case in all the structures we studied. We have verified in the eigenenergies that the replacement of $m_{\|}(z,E_i^{(0)})$ by $m'^*(z)$ in Eq. (18) makes negligible difference because the second term in the numerator is already a small correction (of the order a few percent) of unity in the first term and the energy dependence in $m_{\|}(x,E_i^{(0)})$ provides a small correction to $m'^*(z)$. The wave function ψ_i tends to confine the electron to the well region where $E_i - V(z) + \delta V_b$ is small. In this case, the Schrödinger-like effective-mass equation including strain effects becomes

$$\left[-\frac{1}{2}\frac{d}{dz}\frac{1}{m_{\|}(z,E_i^{(0)})}\frac{d}{dz} + V(z) - E_i^{(0)}\right]\psi_i = 0. \tag{19}$$

The mobile electron density becomes

$$\rho(z) = \sum_i N_i \psi_i^2, \tag{20a}$$

$$N_i = \frac{m_i^*}{\pi} kT \ln\left(1 + \exp\frac{E_F - E_i^{(0)}}{kT}\right), \tag{20b}$$

$$m_i^* = \frac{1 + \frac{1}{4}\left\langle \frac{d\psi_i}{dz} \left| \frac{1}{m'^*(z)\Delta'(z)} \right| \frac{d\psi_i}{dz} \right\rangle}{\left\langle \psi_i \left| \frac{1}{m_{\perp}(z,E_i^{(0)})} \right| \psi_i \right\rangle}. \tag{20c}$$

The self-consistent problem consists in solving Eqs. (19) and (11) with $V(z)$ given by Eq. (10) and $\rho(z)$ by Eq. (20). We have solved this problem numerically. First we solve Eq. (19) using the finite-difference method; we start by setting $E_i^{(0)}$ to zero in the mass term. Then we solve the problem iteratively updating the mass with the new value of $E_i^{(0)}$. Once the eigenvalues and the corresponding eigenvectors are obtained, we solve the Poisson equation with the appropriate boundary conditions to find the Hartree energy and the Fermi energy. To update $V(z)$ for the next iteration in the self-consistent procedure, we have used Broyden's method,[21] which we found to converge faster than any other method based on the simple mixing scheme.

C. *DX* centers

As mentioned in the Introduction, when doping impurities of group IV are introduced in some III-V semiconductors as donors, they are found to exhibit the persistent photoconductivity (PPC) phenomenon. This effect can be explained by deep donor levels called DX centers.[10] It is now accepted that the model proposed by Chadi and Chang[13] is adequate to describe the donors. Therefore we will use that model to calculate their statistics. The defects are assumed to have three charge states, (1) a shallow neutral state, doubly degenerate, with an ionization energy E_{d_1}, (2) a nondegenerate, positively ionized state, with the electron released to the conduction band, and (3) a deep state negatively charged, with a degeneracy factor of 4, coming from the four possible <111> directions that the impurity has to go to the interstitial position, and an ionization energy E_{d_2}. We used the grand canonical ensemble to derive the occupation distribution of the defect.[22] In the limit of high doping densities where the shallow level merges with the ionized band, the total charge of the center is[23]

$$\rho_d(z) = N_d(z)\frac{1 - 4\exp[\beta(2E_F - E_{d_1} - E_{d_2})]}{1 + 4\exp[\beta(2E_F - E_{d_1} - E_{d_2})]}, \tag{21}$$

where E_F is the Fermi energy, $N_d(z)$ is the intended doping density profile of the Si donors, and $\beta = 1/kT$, k being the Boltzmann constant and T the temperature.

III. *C-V* CALCULATION

In this section we describe a way to calculate the capacitance of the heterostructures which avoids numerical differentiation with respect to the gate voltage by a self-consistent first-order perturbative treatment of the change of the self-consistent bands as the gate voltage varies. The capacitance is given by

$$C_V = \frac{\delta Q}{\delta V_g}, \tag{22}$$

where V_g is the gate voltage and Q the total electronic charge which is given by

$$Q = \sum_i N_i. \tag{23}$$

Since the capacitance is measured by placing the sample between an Ohmic contact and a Schottky barrier we have to use the boundary conditions described at the end of section II A. The energy at the top of the Schottky barrier is given by[24]

$$V_0 = \Phi_b + E_F - V_g, \tag{24}$$

where Φ_b is the Schottky-barrier height of the metal semiconductor contact. The relation is made clear by an example studied later in Fig. 4. We also express the solution of Eq. (11) using the Green's function for the Poisson equation in one dimension

$$G(z,z') = \int_z^{z'} \frac{dz''}{\epsilon(z'')} \tag{25}$$

as

$$V_H(z) = 4\pi \int G(z,z')[\rho_d(z') - \rho(z')]dz'. \tag{26}$$

By differentiation of Eq. (23) we get

$$\begin{aligned}\delta Q &= \sum_i \delta N_i \\ &= \sum_i \left\{ \frac{\delta m_i^*}{\pi} kT \ln\left(1 + \exp\frac{E_F - E_i^{(0)}}{kT}\right) \right. \\ &\quad \left. + \frac{m_i^*}{\pi} f(E_i^{(0)})\delta(E_F - E_i^{(0)}) \right\}. \end{aligned} \tag{27}$$

A change in the applied gate voltage leads to a change in the self-consistent potential $\delta V(z)$, which leads to a change in the electronic states $\delta E_i^{(0)}$ and corresponding wave functions $\delta\psi_i$. We can use the first-order perturbation theory to express $\delta E_i^{(0)}$ and $\delta\psi_i$ in terms of the matrix elements of

$$\delta V(z) = \delta V_H(z) + \delta V_{\rm XC}(z) \tag{28}$$

between the eigenstates of the effective-mass equation (19). The problem now is to determine these matrix elements

$$V_{ij} = \langle\psi_i|\delta V_H + \delta V_{\rm XC}|\psi_j\rangle \tag{29}$$

which in turn depend on the change in density and to determine the change in the Fermi energy in terms of δV_g. To do this we rewrite the two terms in Eq. (28) as

$$\delta V_H(z) = -4\pi \int G(z,z')\delta\rho(z')dz', \tag{30a}$$

$$\delta V_{\rm XC}(z) = \frac{\partial V_{\rm XC}(\rho(z))}{\partial\rho(z)}\delta\rho(z). \tag{30b}$$

We can also write the change in the Fermi energy by using Eq. (24) as

$$\delta E_F = \delta V_g - 4\pi \int G(0,z)\delta\rho(z)dz. \tag{31}$$

We again use first-order perturbation theory[25] to express the change in the electronic density as a function of V_{ij} and substitute it in the previous three equations. Using Eq. (31) to express δE_F in terms of V_{ij} in Eq. (30) we obtain an integral equation with a separable kernel for $\delta V_H(z)$ and $\delta V_{\rm XC}(z)$. By taking the matrix elements of both sides of these equations between the eigenstates of Eq. (19), we obtain a linear system of equations for those matrix elements. By solving this system for V_{ij} in terms of δV_g and substituting in Eq. (27) we obtain the desired result for C_V.

IV. RESULTS FOR THREE HETEROSTRUCTURES

Based on the model with the ingredients described in Sec. II, we have written a computer program which is flexible enough to study the electronic properties as a function of the heterostructure configuration at any temperature. In this section we present the results for three different classes of configurations. Table I summa-

TABLE I. Parameters used in the self-consistent calculation.

Parameter[a]	GaAs	InAs	AlAs
E_g (eV)	$1.519 - \frac{5.408\times10^{-4}T^2}{T+240}$	0.418	3.13
m^* (m_0)	0.067	0.0239	0.15
ϵ	$12.40(1+1.2\times10^{-4}$ T)	15.15	10.06
a (eV)	−9.80	−6.00	–
b (eV)	−1.70	−1.80	–
d (eV)	−5.30	−3.60	–
C_{11} (10^{11} dyn/cm^2)	11.26	8.329	12.02
C_{12} (10^{11} dyn/cm^2)	5.57	4.526	5.70
C_{44} (10^{11} dyn/cm^2)	6.00	3.959	5.89
a (Å)	5.653	6.0583	5.66

[a]From Ref. 26.

rizes the input parameters for the three bulk compounds, GaAs, InAs, and AlAs, used in the calculations. For the ternary compounds, we take the linear interpolation from the parameters of the binary compounds, except for the band gaps where we take[26]

$$E_g(\mathrm{Al}_y\mathrm{Ga}_{1-y}\mathrm{As}) = E_g(\mathrm{GaAs}) + 1.087y + 0.438y^2, \tag{32a}$$

$$E_g(\mathrm{In}_x\mathrm{Ga}_{1-x}\mathrm{As}) = E_g(\mathrm{GaAs}) - 1.5837x + 0.375x^2. \tag{32b}$$

A. Single δ layer in GaAs

The simplest application of our theory is to a single δ layer of Si impurities embedded in GaAs. The electron subbands have been calculated before.[27] We repeat the calculation using our model to find the occupation density of each subband, which can be compared to experimental Shubnikov–de Haas measurements, in order to assess the accuracy of our model. In Fig. 1 we present the occupation density in each subband as a function of the impurity concentration in the doping layer at a temperature $T = 4.2$ K. For doping density N_d=6.7×10^{12} cm^{-2}, a comparison with available experimental results[27] can be made. Table II contains the measured subband densities and the corresponding calculated values for one-band and two-band models. We have in addition included the effect of a finite spread dz of the doping layer up to 40 Å.[27] Comparison with experiment shows that the improvement of the two-band model over the one-band model is of the same order as the finite extent of the doping layer at 40 Å. We also note that the results are insensitive to a spread of the doping layer which is less than the quantum-mechanical width of the channel electron-density profile (i.e., approximately between 0 Å and 20 Å), in which case the δ model can be used. Figure 2 is the room-temperature C-V curve for a structure with a density of 5×10^{12} cm^{-2} located 600 Å from the surface of the sample. Like the parabolic quantum well, the single δ-layer system has multiple subband occupation which can easily be changed by the application of gate voltage. The C-V curve does not show any structure due to the depopulation of the subbands as the gate voltage is increased.

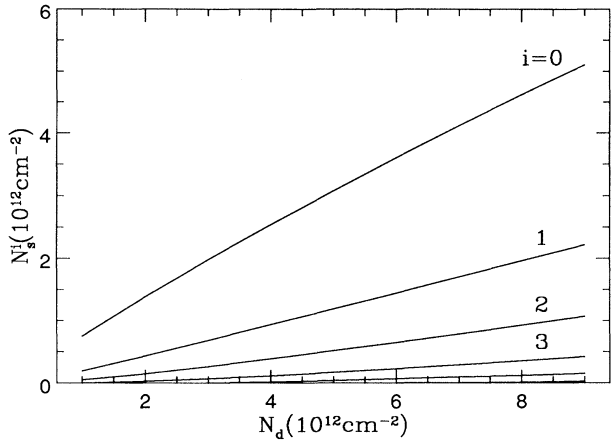

FIG. 1. Subband occupation as a function of δ-doping donor concentration for δ-doped GaAs.

B. δ-modulation-doped asymmetric quantum wells

Here we wish to consider the δ-doped layer as a source located in the barrier region for providing carriers in the well region. This is the prototype for an electronic device. We are particularly interested in how high a carrier density can be achieved. This is not simply a question of increasing the doping density. There are limiting factors such as the confining potential due to the band-edge offset and the creation of a second channel in the doping region. To these factors, we add the problem of the DX centers providing deep donor levels which are not easily ionized. As an example with experimental relevance, we present theoretical results for an $\mathrm{Al}_y\mathrm{Ga}_{1-y}\mathrm{As}/\mathrm{In}_x\mathrm{Ga}_{1-x}\mathrm{As}/\mathrm{GaAs}$ single asymmetric quantum well. The well material is chosen to be $\mathrm{In}_x\mathrm{Ga}_{1-x}\mathrm{As}$ to increase the confining band-edge offset and to provide a variation on the well-studied GaAs well.

TABLE II. Comparison between the Shubnikov–de Haas values of the occupation densities for each subband and the one- and two-band model calculations.

Subband	Expt.[a]	One-band (dz=0)		Two-band (dz=0)		Two-band (dz=20 Å)		Two-band(dz=40 Å)	
i	N_i^b	E_i^c	N_i	E_i	N_i	E_i	N_i	E_i	N_i
0	3.83	−146.9	4.12	−137.4	3.97	−136.6	3.94	−133.2	3.83
1	1.74	−57.3	1.61	−55.5	1.63	−56.1	1.64	−58.5	1.71
2	0.76	−25.6	0.72	−25.7	0.75	−25.8	0.75	−26.2	0.76
3	0.29	−8.3	0.23	−9.5	0.27	−.6	0.28	−10.2	0.29
4	—	−1.4	0.04	−3.1	0.088	−3.1	0.089	−3.3	0.092

[a]From Ref. 27.
[b]All occupation densities are in 10^{12} cm^{-2}.
[c]Subband energies are in meV and measured from the Fermi level.

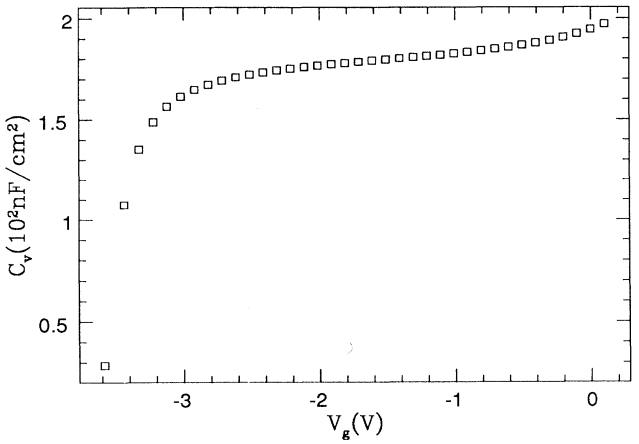

FIG. 2. Self-consistent capacitance vs applied voltage for δ-doped GaAs. The points are obtained from the self-consistent calculation as outlined in Sec. III.

The system is grown in the [001] direction with the following dimensions: 1000 Å of undoped GaAs, followed sequentially by an active layer of $In_xGa_{1-x}As$ of width W_d, a spacer layer of undoped $Al_yGa_{1-y}As$ of width s, a Si δ-doping layer of variable density N_d, and finally an 800-Å layer of undoped $Al_yGa_{1-y}As$. First we chose an active channel of width 100 Å, a spacer of 100 Å, and studied the electronic density in the channel as a function of N_d. We took x=0.17, y=0.35, T = 1.6 K, a conduction-band offset of 70% of the strained band-gap difference, a surface potential of 0.7 V to account for an n^{++} GaAs cap layer, and the deep donor level $E_{d_2}=2\times(0.7y-0.15)$ eV.[28] The results are shown in Fig. 3. We see that the electronic density in the channel saturates due to the presence of the DX centers in the $Al_{0.35}Ga_{0.65}As$ layer. As the density of Si donors increases, the fraction of doubly occupied states rises to a saturation limit giving a maximum active channel density of 1.397×10^{12} cm^{-2}.

This is reminiscent of the observation of Ref. 29 where it was suggested that the free-electron concentration in δ-doped GaAs may saturate when the depth of the potential is such that the Fermi energy coincides with the energy level of the DX center. This would occur at a critical value of 5.5×10^{12} cm^{-2}. Figure 4 shows a typical self-consistent potential and electronic density. In order to study this saturation phenomenon further, we considered the effect of gate voltage on a similar structure with a well width of 150 Å and a δ-doping layer of density 2.5×10^{12} cm^{-2}. Figure 5 shows the calculated self-consistent channel density and capacitance as a function of applied voltage. The saturation of the channel density due to DX centers is clearly seen. This density remains constant down to a gate voltage of -1.4 V. Below this voltage the capacitance of the structure calculated by the method of Sec. III is due entirely to the charges trapped in the DX centers in the δ-doping layer in the barrier which get depleted first. The structure acts essentially as a plane capacitor. As the reverse gate voltage is increased, the deep centers continue to be depleted until they are empty. When the channel electrons start to get depleted the capacitance shows a discontinuity which indicates that the depleted charges are coming from the channel.

Next we considered the value of the saturation density as a function of configuration. First, we varied y, the Al fraction in the barrier in the range where the deep levels of the DX centers played a major role. Table III shows the saturation density possessing a weak dependence on y. For $y < 0.22$ where the DX center deep levels did not play an essential role at low temperatures, the barrier potential was so low that not all donor electrons left the doping layer. Second, we added a second δ-doping layer on the same side of the barrier keeping the spacer thickness s between the channel and the first δ-doping layer constant.[12] Of course, we could obtain higher channel density by adding the second δ-doping layer to the opposite side of a narrow well or by adding the second δ-doping

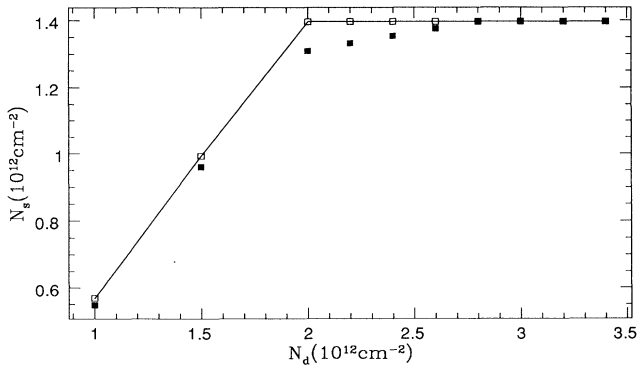

FIG. 3. The channel electron density for $Al_{0.35}Ga_{0.65}As/In_{0.17}Ga_{0.83}As/GaAs$ (900Å/100 Å/1000Å) grown along the [001] axis saturates as the concentration of δ donors is increased. Open squares are for a one δ layer with the lines through them as a guide for the eye and the full squares are for a structure with two δ layers which saturate slower than the former.

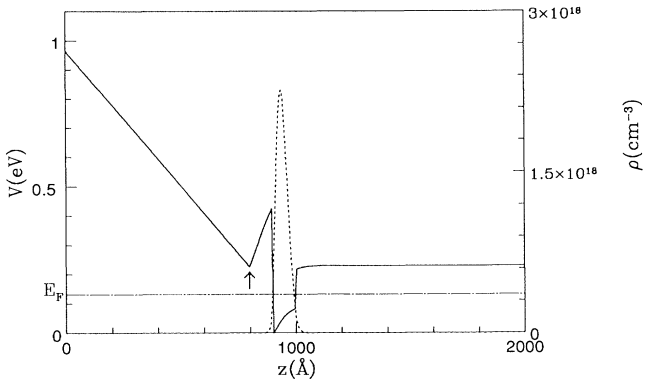

FIG. 4. Typical self-consistent potential (solid line) and electronic density (dashed line) for a $Al_{0.35}Ga_{0.65}As/In_{0.17}Ga_{0.83}As/GaAs$ (900Å/100Å/1000 Å) system grown along the [001] axis. The δ-doping layer of concentration $N_d=2\times10^{12}$ cm^{-2} is located at the position of the arrow in the barrier. We have $V_0 - F_F = \Phi_b - V_g$.

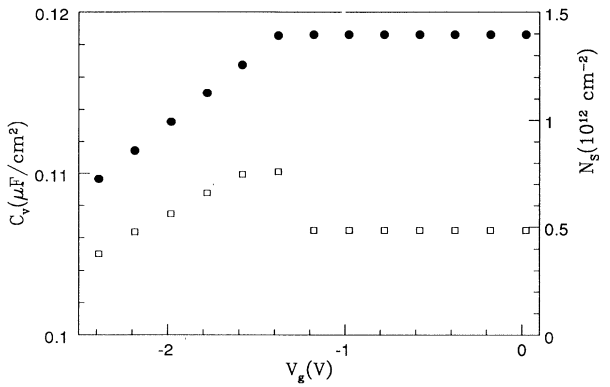

FIG. 5. The filled circles represent the channel electron density for a structure similar to the one described in Fig. 3 with a well width of 150 Å. As the reverse gate voltage is increased it remains constant since the doubly occupied impurity levels are being depleted. The self-consistent capacitance of the structure (open squares) is constant. Once the voltage starts to deplete the channel electrons, the capacitance shows a discontinuity.

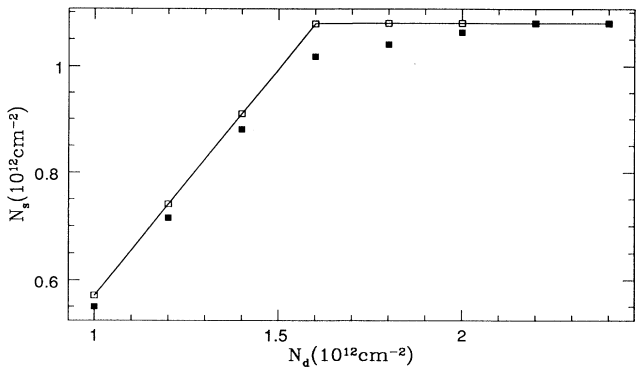

FIG. 6. Same as Fig. 3 except the growth direction is along the [111] axis. We observe a similar result with a much lower value of the saturation density.

layer on the same side but closer to the well. What we wish to test is the variation of the doping structure from one layer to two keeping the spacer distance constant. The addition of the second δ-doping layer under the specified condition did not change the saturation value of the channel electron density although the approach to saturation is slower (Fig. 3). We found that the saturation value did not change even when we varied the separation of the two δ-doping layers provided that s was kept constant. Finally, we found that the saturation was also virtually independent of the width of the quantum-well channel between 100 Å and 150 Å. We have also examined a similar heterostructure grown in the [111]. Figure 6 shows that we obtained a lower saturation value of the channel density of 1.08×10^{12} cm^{-2}.

In this model we neglected the interface traps at the $Al_yGa_{1-y}As/In_xGa_{1-x}As$ interface because their concentration is low[30] compared to the δ concentrations we are using in our study. The channel saturation density can also be affected by compensation effects of the doping impurities in the barrier. This effect depends on the growth conditions and the concentration of the dopants. If we assume that the spread of the doping impurities in the δ-doping layer is of the order of 40 Å then their three-dimensional concentration is intermediate between two regimes identified in Ref. 31 for bulk GaAs where the compensation effects become important from one regime to the other. We, therefore, rely on Ref. 29, which found that for a two-dimensional impurity concentration of 5.7×10^{12} cm^{-2} in GaAs, compensation was not important, to conclude that in our systems the DX centers are the main source of the saturation. This is because the concentrations we are using are lower than this value. Therefore the values we quote here should be considered as upper limits for the saturation densities. In Table IV we compare our theoretical results with Shubnikov–de Haas measurements taken from Ref. 32 for a variety of configuration parameters. The theoretical results are generally in reasonable agreement with the experimental measurement, considering that the experimental error is about 10% and that the remaining discrepancy may be due to minor factors, such as interface traps and the nonideal surface structure, which are not taken into account by our theory. The theory has found no change in the density between two systems with one and two δ layers whereas experiment has found a decrease. This could partly be due to the experimental difficulty of controlling the spread of the first δ layer when the growth is interrupted to insert the second δ layer and partly due to the possibility of two-channel conduction[33] in the one δ-layer but not in the two δ-layer system.

We have also studied heterostructures composed of other semiconductor materials. The lattice-matched $In_{0.52}Al_{0.48}As/In_{0.53}Ga_{0.47}As/InP$ asymmetric quantum well is of device interest. If we take Si-doped $In_{0.52}Al_{0.48}As$ to have centers,[34] and consider a structure with the same dimensions as the structure described above, we find a channel density saturation value

TABLE III. Saturation density as a function of Al content in the barrier.

y	0.25	0.3	0.35
N_S (10^{12} cm^{-2})	1.324	1.357	1.397

TABLE IV. Comparison between the theoretical occupation densities in each subband of the channel electrons with the ones measured by Shubnikov–de Haas. The width of the well is 150 Å, N_d=3.6×10^{12} cm^{-2} and T=1.6 K.

s (in Å)	Expt.[a] N_i [b]	Theory N_i
50	2.29	1.936
	0.293	0.224
100 (one δ layer)	1.53	1.394
100 (two δ layers)	1.33	1.394
200	0.793	0.823

[a]From Ref. 32.
[b]All occupation densities are in 10^{12} cm^{-2}.

of 1.48×10^{12} cm^{-2}, which is slightly higher than the $Al_{0.35}Ga_{0.65}As/In_{0.17}Ga_{0.83}As/GaAs$ system.

C. Parabolic quantum well

To demonstrate the range of applicability of our method to heterostructures, we studied a parabolic well of $Al_xGa_{1-x}As$ where x was varied from 0 at the center of the well to 0.2 at the wall in such a manner to produce a parabolic well. For simplicity we used the one-band model. The width of the well was taken to be 2000 Å. Two symmetric barriers of $Al_{0.3}Ga_{0.7}As$ and width 2250 Å were placed on either side of the well with a doping of density 3×10^{17} cm^{-3} and width 50 Å placed 200 Å from the well. For this parabolic well, we took a linear interpolation for the band gap of $Al_xGa_{1-x}As$, a conduction-band offset of 60% of the band-gap difference and a temperature of 4.2 K. Figure 7(a) shows our self-consistent potential and density for a parabolic quantum well and Fig. 7(b) for a parabolic quantum well with a superimposed superlattice with an Al mole fraction difference of 0.1 between the well and the barrier.[16] In this calculation we allowed both the mass and the dielectric constant to be position dependent. Figures 8(a) and 8(b) show the capacitance per unit area versus applied voltage calculated by the method of Sec. III corresponding to the two parabolic wells. The smooth capacitance curve of Fig. 8(a) shows the absence of structure due to emptying out of subband occupations, contrary to the interpretation of the observed structures in Ref. 15. The steplike changes in the capacitance curve in Fig. 8(b) for the quantum well with a superlattice supports the interpretation of Ref. 16 that these structures are reflections of the spatial inhomogeneities in the electronic charge density.

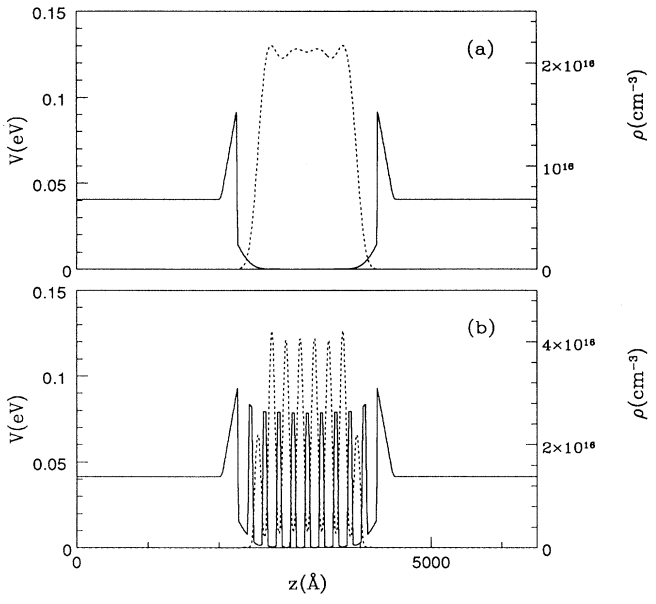

FIG. 7. Self-consistent conduction-band-edge profile (solid line) and density (dashed line) for a parabolic quantum well (a) and for a parabolic quantum well with a superlattice superimposed (b).

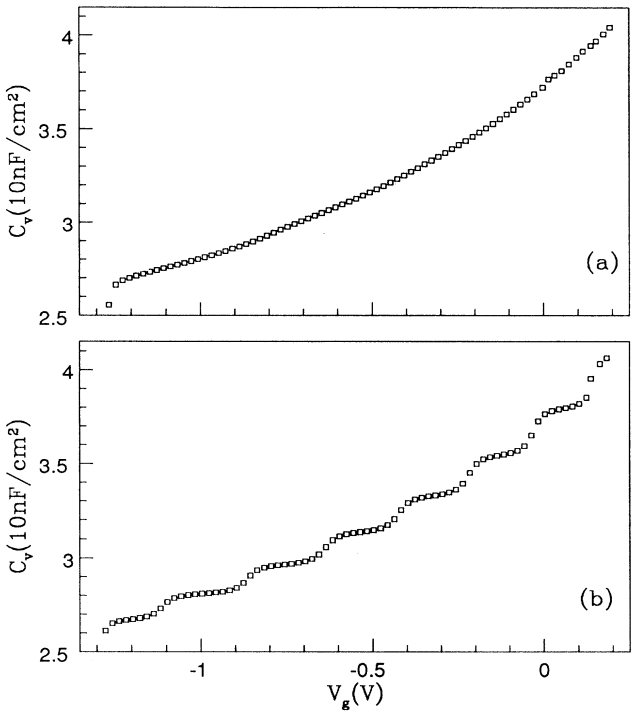

FIG. 8. Self-consistent capacitance vs voltage curve for the parabolic quantum well (a) and for a parabolic quantum well with a superlattice superimposed. The curve in (a) is smooth, similar to the δ-layer curve for δ-doped GaAs of Fig. 2, but the curve in (b) presents steplike changes due to the superimposed superlattice.

V. DISCUSSIONS

In order to have the capability to study the dependence on the configuration of an electronic structure in a semiconductor heterostructure as a guide for device design, we have presented a theoretical model of sufficient flexibility and accuracy. The flexibility is shown by its applicability at any temperature and by the actual computation on three different classes of structures of III-V compounds, two of which include δ layers and one digital alloys. The accuracy necessary is achieved by using the two-band effective-mass approximation, by including strain effects due to lattice mismatch, by adopting the deep donor level model for the DX centers when necessary, and by treating changes due to the variation of gate-voltage analytically.

Study of the specific cases leads us to a number of conclusions of importance for device applications of the heterostructures. Perhaps the foremost is that inclusion of the deep levels of the DX centers leads to a prediction of channel electron-density saturation as the δ-doping layer concentration is increased with a characteristic discontinuity in the capacitance versus voltage curve. While it is obvious that deep level donors will prevent complete

ionization of the donors, it is not clear *a priori* whether the channel carrier density will increase with the doping density or whether it will saturate. We have given saturation density values which can be tested experimentally. The limit of carrier density of a few times 10^{12} cm^{-2} puts a limitation on improving device performance in this direction. We are exploring ways in collaboration with experimentalists[33] both to confirm the saturation effect due to DX centers (in contrast to other causes) and to remove such limitations by placing the DX centers in a thin layer of a compound with no DX centers.[35] A number of phenomena which arise will be reported elsewhere.[33] Another direction to attempt to raise the carrier density is to change the δ-doping structure. A heterostructure with two δ layers on the same side with the same spacer distance from the well as one δ layer is shown to yield the same saturation density. Three δ layers begin to behave like uniform doping.

Analytic formulation of the capacitance leads to reliable calculated differential capacitance dependence on gate voltage. Thus, theory is able to help show that structures in the C-V curves reflect spatial charge inhomogeneities but not the emptying of electron subbands.

The easy applicability of our model to a wide range of III-V semiconductor heterostructures provides the possibilities for innovative designs and for new studies of the electronic properties. In addition to the above-mentioned collaboration with experimentalists to explore the theoretical consequences of placing the doping layers in an environment free of DX centers, we have explored the theory of using superlattices as elements of the heterostructure[36] and we have started a collaboration to understand the electron-spin transport across a Schottky barrier built on heavily doped silicon[37] and to understand the theoretical basis of the δ-doped Ohmic junction.[38]

ACKNOWLEDGMENTS

This work was supported by NSF Grant No. DMR 91-17298 and No. NSF I/UCRC. We thank Professor H. H. Wieder and J. M. Fernández for stimulating discussions and permission to quote their experimental results prior to publication. L. J. Sham is grateful to Dr. Thomas Theis for helpful discussions on the DX centers.

[1] C. T. Foxon and B. A. Joyce, *Fundamental Aspects of Molecular Beam Epitaxy,* in Current Topics in Material Science Vol. 7, edited by E. Kaldis (North-Holland, Amsterdam, 1981).
[2] C. E. C. Wood, G. M. Metze, J. D. Berry, and L. F. Eastman, J. Appl. Phys. **51**, 383 (1980).
[3] E. F. Schubert, J. Vac. Sci. Technol. A **8**, 2980 (1990).
[4] C. Weisbuch and B. Vinter, *Quantum Semiconductor Structures* (Academic, San Diego, 1991).
[5] G. Brozak, E. A. de Andrada e Silva, L. J. Sham, F. DeRosa, P. Miceli, S. A. Schwarz, J. P. Harbison, L. T. Florez, and S. J. Allen, Jr., Phys. Rev. Lett. **64**, 471 (1990), and references therein.
[6] E. O. Kane, in *Physics of III-V Compounds*, edited by R. K. Willardson and A. C. Beer (Academic, New York, 1966), Vol. 1.
[7] W. Kohn and L. J. Sham, Phys. Rev. **140**, A1133 (1965).
[8] G. C. Osbourn, P. L. Gourley, I. J. Fritz, R. M. Biefeld, L. R. Dawson, and T. E. Zipperian, in *Applications of Multiquantum Wells, Selective Doping, and Superlattices*, edited by R. Dingle (Academic, New York, 1987); Semiconductors Semimetals **24**, 459 (1987).
[9] D. V. Lang and R. A. Logan, Phys. Rev. Lett. **39**, 635 (1977).
[10] P. M. Mooney, J. Appl. Phys. **67**, R1 (1990).
[11] A. Kumar, S. E. Laux, and F. Stern, Phys. Rev. B **42**, 5166 (1990).
[12] H. Tian, K. W. Kim, and M. A. Littlejohn, J. Appl. Phys. **70**, 4593 (1991).
[13] D. J. Chadi and K. J. Chang, Phys. Rev. Lett. **61**, 873 (1988).
[14] S. Wang, *Fundamentals of Semiconductor Theory and Device Physics* (Prentice-Hall, Englewood Cliffs, NJ, 1989), p. 526.
[15] A. Wixforth, M. Sundaram, K. Ensslin, J. H. English, and A. C. Gossard, Appl. Phys. Lett. **56**, 454 (1990).
[16] M. Sundaram, A. Wixforth, P. F. Hopkins, and A. C. Gossard, J. Appl. Phys. **72**, 1460 (1992).
[17] F. Pollak and M. Cardona, Phys. Rev. **172**, 816 (1968).
[18] J. P. Perdew and A. Zunger, Phys. Rev. B **23**, 5048 (1981).
[19] D. L. Smith and C. Mailhiot, J. Appl. Phys. **63**, 2717 (1988).
[20] G. Bastard, *Wave Mechanics Applied to Semiconductor Heterostructures* (Edition de Physique, Les Ulis, France, 1988).
[21] G. P. Srivastava, J. Phys. A **17**, L317 (1984).
[22] W. Shockley and J. T. Last, Phys. Rev. **107**, 392 (1957).
[23] T. Suski, R. Piotrzkowski, P. Wiśniewski, E. Litwin-Staszewska, and L. Dmowski, Phys. Rev. B **40**, 4012 (1989).
[24] M. B. Patill and H. Morkoç, Solid State Electron. **33**, 99 (1990).
[25] H. Ehrenreich and M.H. Cohen, Phys. Rev. **115**, 786 (1959).
[26] Author, in *Numerical Data and Functional Relationships in Science and Technology*, Landolt-Börnstein, New Series, Vol. III, New Series, edited by O. Madelung (Springer-Verlag, Berlin, 1987).
[27] A. Zrenner, F. Koch, and K. Ploog, Surf. Sci. **196**, 671 (1988).
[28] D. J. Chadi and K. J. Chang, Phys. Rev. B **39**, 10063 (1989).
[29] A. Zrenner, F. Koch, R. L. Williams, R. A. Stradling, K. Ploog, and G. Weinmann, Semicond. Sci. Technol. **3**, 1203 (1988).
[30] D. J. As and P. W. Epperlein, J. Appl. Phys. **64**, 2408 (1988).
[31] J. Maguire, R. Murray, R. C. Newman, R. B. Beall, and R. C. Harris, Appl. Phys. Lett. **50**, 516 (1987).
[32] J. M. Fernández and H. H. Wieder (unpublished).
[33] J. M. Fernández, M. E. Lazzouni, L. J. Sham, and H. H. Wieder, J. Appl. Phys. (to be published).
[34] K. Nakashima, S. Nijima, Y. Kawamura, and H. Asahi, Phys. Status Solidi A **103**, 511 (1987).

[35] C. W. Tu, W. L. Jones, R. F. Kopf, L. D. Urbanek, and S. S. Pei, IEEE Electron. Device Lett. **EDL-7**, 552 (1986) and references therein.
[36] M. E. Lazzouni, G. Einevoll, and L. J. Sham, J. Appl. Phys. (to be published).
[37] J. Anderberg, Ph.D. thesis, University of California, San Diego, 1992.
[38] M. Missous, in *GaAs and Related Compounds, Seattle, 1991*, edited by G. B. Stringfellow (Institute of Physics, Bristol, 1991), p. 187.